

Kelvin-Helmholtz Instability and Circulation Transfer at an Isotropic-Anisotropic Superfluid Interface in a Neutron Star

A. Mastrano^{1*} and A. Melatos^{1†}

¹*School of Physics, University of Melbourne, Parkville VIC 3010, Australia*

Accepted ?. Received ?; in original form ?

ABSTRACT

A recent laboratory experiment (Blaauwgeers et al. 2003) suggests that a Kelvin-Helmholtz (KH) instability at the interface between two superfluids, one rotating and anisotropic, the other stationary and isotropic, may trigger sudden spin-up of the stationary superfluid. This result suggests that a KH instability at the crust-core (1S_0 - 3P_2 -superfluid) boundary of a neutron star may provide a trigger mechanism for pulsar glitches. We calculate the dispersion relation of the KH instability involving two different superfluids including the normal fluid components and their effects on stability, particularly entropy transport. We show that an entropy difference between the core and crust superfluids reduces the threshold differential shear velocity and threshold crust-core density ratio. We evaluate the wavelength of maximum growth of the instability for neutron star parameters and find the resultant circulation transfer to be within the range observed in pulsar glitches.

Key words: dense matter – hydrodynamics – instabilities – pulsars: general – stars: interiors – stars: neutron

1 INTRODUCTION

It has been proposed that the neutrons making up the inner crust and core of a neutron star display superfluid-like behaviour (Tamagaki 1970; Yakovlev, Levenfish & Shibano 1999). They are compressed to such a high density that they act like composite bosons, forming Bardeen-Cooper-Schrieffer (BCS) pairs which condense into the ground state below a critical temperature T_c and behave like terrestrial superfluids (e.g. ^4He). Calculations of the pair interaction and energy gap suggest that different types of Cooper pairs populate the crust and the core of a neutron star, 3P_2 (triplet) pairs in the core and 1S_0 (singlet) pairs in the crust (Hoffberg et al. 1970; Tamagaki 1970; Baym & Pethick 1975; Brand & Pleiner 1981; Yakovlev, Levenfish & Shibano 1999; Khodel, Khodel & Clark 2001). Superfluidity enhances neutron star cooling, reduces the heat capacity of the star, and suppresses neutrino emission (Yakovlev, Levenfish & Shibano 1999; Tsuruta et al. 2001). In addition, pulsar glitches (discontinuous spin-up events) are attributed to the motion of superfluid vortex lines; these lines tend to be pinned to the nuclei in the stellar crust and sudden, large-scale creep of these lines from one pinning site to another may be responsible for glitches (Link, Epstein & Baym 1993)

Macroscopic phase coherence endows a superfluid with frictionless flow and irrotationality (Putterman 1974; Tilley & Tilley 1994; Khalatnikov 2000; Vollhardt & Wölfle 2002). Irrotationality leads to formation of discrete quantized vortices if the fluid rotates. This behaviour is well known and observed in terrestrial samples of superfluid ^4He (Putterman 1974; Tilley & Tilley 1994). Landau (1941) put forth what is known as the two-fluid model (where ^4He is modelled as two separate components, the inviscid superfluid and the viscous normal fluid) to explain the various phenomena observed in superfluid flows such as second sound (an entropy-temperature wave, where the two components move in opposite directions, induced by

* E-mail: a.mastrano@physics.unimelb.edu.au

† E-mail: a.melatos@physics.unimelb.edu.au

a temperature gradient) and the fountain effect (Putterman 1974; Khalatnikov 2000). This hydrodynamic model is successful and has been polished to a high degree of sophistication, taking into account more and more effects, such as the motion of quantized vortices and the drag forces they exert (Hall & Vinen 1956; Barenghi & Jones 1988). Superfluidity in ^3He , on the other hand, was first observed more recently (Leggett 1975; Wheatley 1975) (see also Lee 1997 for a first-person account of its discovery) and the search for a complete hydrodynamic theory continues; for a comprehensive and up-to-date account, see Vollhardt & Wölfle (2002).

^3He superfluid is a condensate of ^3He Cooper pairs. The generally accepted theory of ^3He superfluidity postulates p -wave pairing with spin angular momentum \hbar and orbital angular momentum \hbar . Experiments show that there are two distinct phases of superfluid ^3He , known as He-A and He-B. He-B occupies the 3P_0 state; it is isotropic and behaves like ^4He superfluid. He-A occupies the 3P_2 state; the axis of the orbital angular momentum defines a preferred direction (generally denoted as $\hat{\mathbf{l}}$), breaking the symmetry of the ground state.¹ This anisotropy manifests itself as a ‘texture’, defined to be the vector field tangent to the local direction of the pair angular momentum (Leggett 1975; Lee 1997; Vollhardt & Wölfle 2002). The texture in the lowest energy state (undisturbed He-A) is uniform, but heat and fluid flows, applied electromagnetic fields, and container walls deform it. The texture, in turn, inhibits flows and heat transport perpendicular to itself. Hence, the presence of textures modifies the characteristics of any flows induced upon the fluid.

A recent laboratory experiment with superposed He-A and He-B in differential rotation (at an interface stabilised by an applied magnetic field) indicates that the Kelvin-Helmholtz (KH) instability at the interface plays a significant role in triggering transfer of circulation from He-A to the initially irrotational He-B, spinning up the He-B sample; this is detected as discrete jumps in nuclear magnetic resonance absorption signals (Blaauwgeers et al. 2003; Volovik 2002). This exciting result suggests that a similar process may occur at the crust-core superfluid interface in a neutron star, with important implications for pulsar glitches.

In Section 2 we present an analysis of the KH instability involving two superposed superfluids, taking as our starting point the two-fluid model, modified for ^3He . Our analysis extends earlier work in two ways: we treat the flow of entropy in the system self-consistently (cf. Volovik 2002) and consider two different superposed fluids (each with its own superfluid and normal fluid components) in relative motion, not the superfluid and normal fluid components of one fluid (Korshunov 2002). In section 3, we apply our KH dispersion relation to the experiment conducted by Blaauwgeers et al. (2003) and to an idealised neutron star model. This work complements an analysis by Andersson, Comer & Prix (2003) of the two-stream instability, a different process involving two interpenetrating, isotropic superfluids, which is also a possible triggering mechanism for glitches.

2 KELVIN-HELMHOLTZ INSTABILITY

2.1 Two-fluid model of ^3He

We restrict our attention to the hydrodynamic regime, where disturbances of the equilibrium are much slower than the typical particle collision time. The nondissipative hydrodynamic equations describing an anisotropic superfluid are (Putterman 1974; Landau & Lifshitz 1987; Vollhardt & Wölfle 2002)

$$\rho_n \left(\frac{\partial v_{n,i}}{\partial t} + \mathbf{v}_n \cdot \nabla v_{n,i} \right) = -\frac{\rho_n}{\rho} \frac{\partial p}{\partial x_i} - s \rho_s \frac{\partial T}{\partial x_i} - \frac{\rho_s \rho_n}{\rho} (\mathbf{v}_{ns} \cdot \nabla) v_{n,i} + \rho_n g_i + \sigma_{n,i} \left(\frac{\partial^2 z'_n}{\partial x^2} + \frac{\partial^2 z'_n}{\partial y^2} \right) \delta(z), \quad (1)$$

$$\rho_s \left(\frac{\partial v_{s,i}}{\partial t} + \mathbf{v}_s \cdot \nabla v_{s,i} \right) = \frac{\rho_s \hbar}{2m} \epsilon_{ijk} \hat{l}_j \frac{\partial \hat{l}_k}{\partial t} \frac{\partial \hat{l}_m}{\partial x_i} - \frac{\rho_s}{\rho} \frac{\partial p}{\partial x_i} + s \rho_s \frac{\partial T}{\partial x_i} + \frac{\rho_s \rho_n}{\rho} (\mathbf{v}_{ns} \cdot \nabla) v_{n,i} + \rho_s g_i + \sigma_{s,i} \left(\frac{\partial^2 z'_s}{\partial x^2} + \frac{\partial^2 z'_s}{\partial y^2} \right) \delta(z), \quad (2)$$

$$\left(\frac{\partial}{\partial t} + \mathbf{v}_n \cdot \nabla \right) \rho_s = 0, \quad (3)$$

$$\left(\frac{\partial}{\partial t} + \mathbf{v}_n \cdot \nabla \right) \hat{l}_i = -\lambda_4 \frac{\hbar \rho_s}{2m} \epsilon_{ijk} \hat{l}_j (\mathbf{v}_{ns} \cdot \nabla) \hat{l}_k, \quad (4)$$

$$\nabla \cdot \mathbf{v}_n = 0, \quad (5)$$

$$\nabla \cdot \mathbf{v}_s = 0, \quad (6)$$

$$\left(\frac{\partial}{\partial t} + \mathbf{v}_n \cdot \nabla \right) \rho_n = 0, \quad (7)$$

$$\left(\frac{\partial}{\partial t} + \mathbf{v}_s \cdot \nabla \right) \rho_s = 0, \quad (8)$$

¹ The experimental identification of the He-A and He-B as anisotropic and isotropic Cooper pair superfluids remains ambiguous (Wheatley 1975; Tang et al. 1991).

$$\left(\frac{\partial}{\partial t} + \mathbf{v}_n|_{z=0} \cdot \nabla\right) z'_n = v'_{n,z}|_{z=0}, \quad (9)$$

$$\left(\frac{\partial}{\partial t} + \mathbf{v}_s|_{z=0} \cdot \nabla\right) z'_s = v'_{s,z}|_{z=0}. \quad (10)$$

The interface is defined to be at $z = 0$, the zeroth order flows are in the x -direction, and the velocities in (9) and (10) are evaluated at the unperturbed interface. In (1)–(10), $\rho_{s,n}$ are the super- and normal fluid densities respectively, \mathbf{g} is the gravitational acceleration (directed towards negative z -axis), $\boldsymbol{\sigma}_{n,s}$ is the surface tension force per unit length for the normal and superfluid interfaces respectively (directed towards the positive z -axis), $z'_{n,s}$ is the perturbed z -coordinate of the normal and superfluid interfaces, p , T , s , and m denote the pressure, temperature, specific entropy, and mass of an individual constituent particle, $\hat{\mathbf{I}}$ is the unit vector tangent to the texture (in other words, along the direction of the pair angular momentum), $\mathbf{v}_{s,n}$ are the superfluid and normal fluid velocities, and $\mathbf{v}_{ns} = \mathbf{v}_s - \mathbf{v}_n$ is the counterflow velocity. Note that there is no unique equation of state relating ρ_s, ρ_n, s, T , and p ; these quantities evolve independently through the heat transfer (energy) equation (3). An isotropic superfluid is a special case, in which one sets $\hat{\mathbf{I}} = 0$ in (1)–(10).

Equations (1) and (2), the equations of motion governing the normal fluid and the superfluid, are modified with respect to a classical fluid by adding the terms $s\rho_s\partial T/\partial x_i$ and $(\rho_s\rho_n/\rho)(\mathbf{v}_{ns} \cdot \nabla)v_{ns,i}$. These terms come from the gradient of the superfluid chemical potential μ . In a classical fluid, one simply has $\nabla\mu = \nabla p$, whereas in a superfluid, the entropy gradient can drive flows separately from the pressure gradient, because entropy is carried only by the normal fluid component. The $s\rho_s\partial T/\partial x_i$ term leads to effects like second sound, a temperature-entropy wave which differs from ‘first sound’, the usual pressure-density wave (Landau 1941). In addition, the first term on the right-hand side of (2) describes the force exerted by the texture in an anisotropic superfluid when the texture is bent; the ground state of the superfluid far from any walls corresponds to uniform $\hat{\mathbf{I}}$ (see Section 2.2), so the texture ‘stiffens’ the system and opposes flows which might bend it (Vollhardt & Wölfle 2002). Equation (3) is our (non-dissipative) equation of entropy transport [as for the electron-and-muon fluid in Mendell (1991)]. Equation (4) describes the evolution of the texture. Bending the texture (i.e. changing the direction of $\hat{\mathbf{I}}$) shifts the energy gap and the momentum distribution of normal fluid excitations, which then reacts back on the texture itself. The term on the right-hand side of (4) derives from the dependence of the free energy density (which is a function of $\partial\hat{l}_i/\partial x_j$) on the superfluid velocity (Vollhardt & Wölfle 2002). The remaining equations are standard: (5) and (6) enforce incompressibility, (7) and (8) enforce mass continuity, and (9) and (10) ensure that no fluid particles cross the interface, i.e. the fluids are immiscible (Chandrasekhar 1961).

For simplicity, we make some approximations. We set all coefficients of conductivity on the right-hand side of (3) to zero. We also neglect the anisotropy in density for flows along and transverse to the texture, and we omit terms involving changes in free energy as the local texture changes, i.e. we postulate that the texture is in thermodynamic equilibrium to the zeroth order. In reality, (2) features a heat current term proportional to ∇T , with the thermal conductivities for flows parallel and perpendicular to $\hat{\mathbf{I}}$ scaling as $\kappa_{\parallel} \sim (T_c/T)\kappa_N(T_c)$ and $\kappa_{\perp} \sim (T/T_c)\kappa_N(T_c)$ respectively, where $\kappa_N(T_c)$ is the (isotropic) conductivity at the critical temperature. Similarly, although the physical density of the fluid at any point is uniquely defined, the anisotropic texture modifies the mass current to become $\rho_{\perp}v$ perpendicular to $\hat{\mathbf{I}}$ and $\rho_{\parallel}v$ parallel to $\hat{\mathbf{I}}$. This counterintuitive property, which arises because the two-fluid description is an effective theory where it is not possible to label individual ^3He atoms as s or n , is more pronounced at lower temperatures, with $\rho_{n\parallel} = \pi^2(m^*/m)(k_B T/\Delta_0)^2\rho$ and $\rho_{n\perp} = (7\pi^4/15)(m^*/m)(k_B T/\Delta_0)^4\rho$ as $T \rightarrow 0$, for example. Here, m^* is the effective mass of each constituent particle and Δ_0 is the maximum gap parameter, the energy needed to excite one pair out of the ground state (Vollhardt & Wölfle 2002).

2.2 Unperturbed interface: uniform texture

We investigate the situation where an isotropic superfluid is superposed on an anisotropic superfluid and moves relative to it with a constant and uniform velocity. We follow the derivation of the dispersion relation of the classical KH instability described by Chandrasekhar (1961), assuming continuous stratification of the fluid variables in the top and bottom layers with a discontinuous jump at the interface. The normal and superfluid components interpenetrate; their surfaces are allowed to oscillate with different amplitudes, but must be in phase with each other.

It is clear that a situation where all the quantities are uniform and constant in time satisfies (1)–(10). We take this equilibrium solution as our starting point. A uniform and constant texture, along with uniform and constant normal fluid velocity, satisfies (4) identically. A nonuniform but constant texture is also possible. In fact, it can be shown that the most energetically favourable texture for a superfluid in a spherical container is one where the texture lines radiate from a singularity on the wall, called a ‘bouquet’, ‘fountain’, or ‘boojum’ (Vollhardt & Wölfle 2002). In this paper we assume a uniform and constant texture without any singularities, as well as uniform and constant fluid velocities.

2.3 Perturbed interface: surface Kelvin-Helmholtz wave

We linearise (1)–(10), and take all perturbed (first order) quantities to be proportional to $\exp(ik_x x + ik_y y - i\omega t)$, assuming that the wavelength of the perturbation is much smaller than the length-scale over which the texture changes. We take all zeroth order quantities (except temperature, which is the same for both fluids) to be constant and uniform except in the z direction, allowing for vertical stratification. The zeroth-order shear velocity is chosen in the x direction. From (2), one can see that, given a spatially uniform zeroth-order texture that is also constant in time, the textural contribution to the momentum flux is of quadratic order and thus negligible. One can now ignore the textural effects on the fluid flows, although the first-order texture still evolves according to (4). Writing $D = \partial/\partial z$, we then obtain

$$i\rho_n^0(-\omega + k_x U_n)u_n + \rho_n^0(DU_n)w_n = \frac{-\rho_n^0}{\rho_n^0 + \rho_s^0}(ik_x)p' - s^0 \rho_s^0(ik_x)\tau - \frac{\rho_s^0 \rho_n^0}{\rho_s^0 + \rho_n^0}[(U_s - U_n)ik_x(u_s - u_n) + (w_s - w_n)D(U_s - U_n)], \quad (11)$$

$$i\rho_n^0(-\omega + k_x U_n)v_n = \frac{-\rho_n^0}{\rho_n^0 + \rho_s^0}(ik_y)p' - s^0 \rho_s^0(ik_y)\tau - \frac{\rho_s^0 \rho_n^0}{\rho_n^0 + \rho_s^0}(U_s - U_n)ik_x(v_s - v_n), \quad (12)$$

$$i\rho_n^0(-\omega + k_x U_n)w_n = \frac{-\rho_n^0}{\rho_n^0 + \rho_s^0}Dp' - s^0 \rho_s^0 D\tau - g\rho_n' - \frac{\rho_s^0 \rho_n^0}{\rho_n^0 + \rho_s^0}(U_s - U_n)ik_x(w_s - w_n) - k^2 \sigma_n z_n' \delta(z), \quad (13)$$

$$i\rho_s^0(-\omega + k_x U_s)u_s + \rho_s^0(DU_s)w_s = \frac{-\rho_s^0}{\rho_n^0 + \rho_s^0}(ik_x)p' + s^0 \rho_s^0(ik_x)\tau + \frac{\rho_s^0 \rho_n^0}{\rho_s^0 + \rho_n^0}[(U_s - U_n)ik_x(u_s - u_n) + (w_s - w_n)D(U_s - U_n)], \quad (14)$$

$$i\rho_s^0(-\omega + k_x U_s)v_s = \frac{-\rho_s^0}{\rho_n^0 + \rho_s^0}(ik_y)p' + s^0 \rho_s^0(ik_y)\tau + \frac{\rho_s^0 \rho_n^0}{\rho_n^0 + \rho_s^0}(U_s - U_n)ik_x(v_s - v_n), \quad (15)$$

$$i\rho_s^0(-\omega + k_x U_s)w_s = \frac{-\rho_s^0}{\rho_n^0 + \rho_s^0}Dp' + s^0 \rho_s^0 D\tau - g\rho_s' + \frac{\rho_s^0 \rho_n^0}{\rho_n^0 + \rho_s^0}(U_s - U_n)ik_x(w_s - w_n) - k^2 \sigma_s z_s' \delta(z), \quad (16)$$

$$(k_x u_{n,s} + k_y v_{n,s}) = iDw_{n,s}, \quad (17)$$

$$i(-\omega + k_x U_{n,s})\rho'_{n,s} = -w_{n,s}D\rho_{n,s}^0, \quad (18)$$

$$i[-\omega + k_x U_{n,s}(z=0)]z'_{n,s} = w_{n,s}(z=0), \quad (19)$$

where $U_{n,s}$ are the zeroth-order shear velocities (in the x direction as defined previously), u, v , and w are the perturbed velocities in the x, y , and z directions, p' is the first order pressure, τ is the first order temperature, ρ' is the first order density, and other quantities with the superscript '0' are of zeroth order. Following Chandrasekhar (1961), we eliminate all first-order quantities except for $w_{n,s}$. Using (11), (12), (14), and (15) we eliminate τ and p' , while $u_{n,s}$ and $v_{n,s}$ are eliminated using (17). We then obtain the bulk fluid equations (equations which are valid away from the interface) from (13) and (16), after using (18) to eliminate $\rho'_{n,s}$ and (19) to eliminate $z'_{n,s}$.

For the bulk fluids, where all zeroth-order velocities are constant and uniform everywhere, one obtains the following equations which are valid throughout the superfluids and normal fluids away from the interface:

$$\begin{aligned} & \frac{\rho_n^0}{\rho^0}D[\rho_s^0(-\omega + k_x U_s)Dw_s - \rho_s^0 k_x(DU_s)w_s] - \frac{\rho_s^0 \rho_n^0}{\rho^0}k_x(U_s - U_n)k^2 w_s \\ & + s^0 \rho_s^0 D\left\{ \frac{\rho_n^0}{s^0 \rho^0} [(-\omega + k_x U_s)Dw_s + k_x(DU_s)w_s + k_x(U_s - U_n)Dw_s - k_x(DU_s - DU_n)w_s] \right\} \\ & = \rho_n^0(-\omega + k_x U_n)k^2 w_n - \frac{\rho_n^0}{\rho^0}D[\rho_n^0(-\omega + k_x U_n)Dw_n - \rho_n^0 k_x(DU_n)w_n] + gk^2(D\rho_n^0) \frac{w_n}{-\omega + k_x U_n} - \frac{\rho_s^0 \rho_n^0}{\rho^0}k_x(U_s - U_n)k^2 w_n \\ & - s^0 \rho_s^0 D\left\{ \frac{\rho_n^0}{s^0 \rho^0} [(-\omega + k_x U_n)Dw_n - k_x(DU_n)w_n - k_x(U_s - U_n)Dw_n + k_x(DU_s - DU_n)w_n] \right\} \\ & - k^4 \sigma_n \left(\frac{w_n}{-\omega + k_x U_n} \right)_{z=0} \delta(z) \end{aligned} \quad (20)$$

and

$$\begin{aligned} & \rho_s^0(-\omega + k_x U_s)k^2 w_s - \frac{\rho_s^0}{\rho^0}D[\rho_s^0(-\omega + k_x U_s)Dw_s - \rho_s^0 k_x(DU_s)w_s] + gk^2(D\rho_s^0) \frac{w_s}{-\omega + k_x U_s} - \frac{\rho_s^0 \rho_n^0}{\rho^0}k_x(U_s - U_n)k^2 w_s \\ & + s^0 \rho_s^0 D\left\{ \frac{\rho_n^0}{s^0 \rho^0} [(-\omega + k_x U_s)Dw_s + k_x(DU_s)w_s + k_x(U_s - U_n)Dw_s - k_x(DU_s - DU_n)w_s] \right\} \\ & - k^4 \sigma_s \left(\frac{w_s}{-\omega + k_x U_s} \right)_{z=0} \delta(z) \end{aligned}$$

$$\begin{aligned}
 &= \frac{\rho_s^0}{\rho^0} D[\rho_n^0(-\omega + k_x U_n) D w_n - \rho_n^0 k_x (D U_n) w_n] - \frac{\rho_s^0 \rho_n^0}{\rho^0} k_x (U_s - U_n) k^2 w_n \\
 &\quad - s^0 \rho_s^0 D \left\{ \frac{\rho_n^0}{s^0 \rho^0} [(-\omega + k_x U_n) D w_n - k_x (D U_n) w_n - k_x (U_s - U_n) D w_n + k_x (D U_s - D U_n) w_n] \right\}. \tag{21}
 \end{aligned}$$

From (20) and (21), we see that, away from the interface, where $U_{n,s}$, $\rho_{n,s}^0$, and s^0 are constant and uniform, w_n and w_s must satisfy

$$\frac{\rho_n^0 \rho_s^0}{\rho^0} k_x (U_s - U_n) (D^2 w_s - k^2 w_s) = \left[\frac{\rho_n^0 \rho_s^0}{\rho^0} k_x (U_s - U_n) - \rho_n^0 (-\omega + k_x U_n) \right] (D^2 w_n - k^2 w_n), \tag{22}$$

and

$$\left[\frac{\rho_n^0 \rho_s^0}{\rho^0} k_x (U_s - U_n) - \rho_s^0 (-\omega + k_x U_s) \right] (D^2 w_s - k^2 w_s) = \frac{\rho_n^0 \rho_s^0}{\rho^0} k_x (U_s - U_n) (D^2 w_n - k^2 w_n). \tag{23}$$

One nontrivial, stratified solution is $w_{n,s}$: $w_{n,B} = N(-\omega + k_x U_{n,B}) e^{-kz}$, $w_{s,B} = S(-\omega + k_x U_{s,B}) e^{-kz}$, $w_{n,A} = N(-\omega + k_x U_{n,A}) e^{kz}$, and $w_{s,A} = S(-\omega + k_x U_{s,A}) e^{kz}$, where the fluids on top (bottom) are labelled with subscript B (A). Another solution, $\omega = k_x U_n \pm (\rho_s^0 / \rho^0)^{1/2} k_x (U_n - U_s)$, describes a wave propagating in the bulk fluid; it does not describe an instability, so we are not concerned with it here.

The zeroth-order quantities (except T , by assumption) jump across the interface. We integrate the equations across the interface to analyse the interfacial waves. Many of the terms in the above equations are of the form $f(z) Dg(z)$, where both $f(z)$ and $g(z)$ are discontinuous functions. Direct integration of such terms is impossible in general (see Appendix A). However, if one assumes all the zeroth-order quantities change over the same length scale ϵ in passing from the top fluid to the bottom fluid, we can integrate (20) and (21) term by term from $z = -\epsilon$ to $z = +\epsilon$ and then squeeze ϵ to zero in a mathematically regular way. One then substitutes the solutions for $(w_{n,s})_{A,B}$ into the integrated (20) and (21) and obtains two equations involving the oscillation amplitudes N and S . The two equations must be compatible, i.e. linearly dependent. The condition for compatibility gives the following dispersion relation for waves at the interface:

$$\begin{aligned}
 0 &= [\rho_{s,B}^0 (-\omega + k_x U_{s,B})^2 + \rho_{s,A}^0 (-\omega + k_x U_{s,A})^2 + gk(\rho_{s,B}^0 - \rho_{s,A}^0) - k^3 \sigma_s] \\
 &\quad \times \left[\frac{gk}{2} (\rho_{s,B}^0 + \rho_{s,A}^0) (\rho_{n,B}^0 - \rho_{n,A}^0) - \frac{k^3}{2} (\rho_{s,A}^0 + \rho_{s,B}^0) \sigma_n + \alpha \gamma \right] \\
 &+ [\rho_{n,B}^0 (-\omega + k_x U_{n,B})^2 + \rho_{n,A}^0 (-\omega + k_x U_{n,A})^2 + gk(\rho_{n,B}^0 - \rho_{n,A}^0) - k^3 \sigma_n] \\
 &\quad \times \left[\frac{gk}{2} (\rho_{n,B}^0 + \rho_{n,A}^0) (\rho_{s,B}^0 - \rho_{s,A}^0) - \frac{k^3}{2} (\rho_{n,A}^0 + \rho_{n,B}^0) \sigma_s + \alpha \beta \right], \tag{24}
 \end{aligned}$$

with

$$\begin{aligned}
 \alpha &= \frac{1}{24} [(s_B + s_A) (\rho_B^0 - \rho_A^0) (\rho_{s,B}^0 - \rho_{s,A}^0) + (s_B - s_A) (\rho_B^0 + \rho_A^0) (\rho_{s,B}^0 - \rho_{s,A}^0) \\
 &\quad + (s_B - s_A) (\rho_B^0 - \rho_A^0) (\rho_{s,B}^0 + \rho_{s,A}^0)] + \frac{1}{8} (s_B + s_A) (\rho_B^0 + \rho_A^0) (\rho_{s,B}^0 + \rho_{s,A}^0), \tag{25}
 \end{aligned}$$

$$\begin{aligned}
 \beta &= \frac{\rho_{n,B}^0}{s_B \rho_B^0} [(-\omega + k_x U_{s,B})^2 - k_x (U_{s,B} - U_{n,B}) (-\omega + k_x U_{s,B})] \\
 &\quad + \frac{\rho_{n,A}^0}{s_A \rho_A^0} [(-\omega + k_x U_{s,A})^2 - k_x (U_{s,A} - U_{n,A}) (-\omega + k_x U_{s,A})], \tag{26}
 \end{aligned}$$

$$\begin{aligned}
 \gamma &= \frac{\rho_{n,B}^0}{s_B \rho_B^0} [(-\omega + k_x U_{n,B})^2 - k_x (U_{s,B} - U_{n,B}) (-\omega + k_x U_{n,B})] \\
 &\quad + \frac{\rho_{n,A}^0}{s_A \rho_A^0} [(-\omega + k_x U_{n,A})^2 - k_x (U_{s,A} - U_{n,A}) (-\omega + k_x U_{n,A})], \tag{27}
 \end{aligned}$$

$$\rho_{A,B}^0 = \rho_{s,A,B}^0 + \rho_{n,A,B}^0.$$

The dispersion relation (24) is a quartic in ω . It is related to the dispersion relation of the classical KH instability as follows. In (24), we have terms involving superfluid and normal fluid quantities, as well as new terms $\alpha\beta$ and $\alpha\gamma$ which involve the ratios of the bulk entropies. If the superfluid and normal fluid interfaces are decoupled, one must treat the interfaces separately using the classical analysis, i.e. excluding (3) and entropy terms in (1) and (2). For example, if either component is negligible, setting either ρ_s^0 or ρ_n^0 satisfies (24) identically, or if the interfaces are allowed to oscillate separately, cross terms like $s \rho_s \partial T / \partial x$ in (1) or $\rho_s \rho_n \mathbf{v}_{ns}$ in (2) are absent. If neither component is negligible but the counterflow tends to zero, setting α to zero in (24) yields the classical limit, where the components essentially move together as a classical fluid and entropy does not affect stability. If neither component is negligible and there is significant counterflow, one must use the two-fluid dispersion relation (24), as there is no classical analogue.

2.4 Instability threshold and entropy effects

2.4.1 Classical KH instability threshold

In order to understand the onset of the superfluid KH instability, we first review the classical case. The KH instability occurs when two superimposed layers of fluids with different densities are in relative motion. When the velocity shear exceed a critical value, the resulting pressure gradient (from Bernoulli's Law) between the peaks and troughs of an interfacial wave overcomes the surface tension and gravity and the mode grows exponentially. In the classical instability, the interface oscillates at a frequency

$$\omega^c = -\frac{k^c(\rho_A U_A + \rho_B U_B)}{\rho_A + \rho_B} \pm \left[\frac{gk^c(\rho_A - \rho_B) + (k^c)^3\sigma}{\rho_A + \rho_B} - \frac{(k^c)^2\rho_A\rho_B(U_A - U_B)^2}{(\rho_A + \rho_B)^2} \right]^{1/2} \quad (28)$$

for wavenumber k^c (bearing in mind that the subscripts A and B denote the bottom and top fluids respectively). Given a particular density and shear velocity profile, the interface is unstable if $\text{Im}(\omega^c) > 0$, which occurs for wave numbers between

$$k_{\min}^c = \frac{\rho_A\rho_B(U_A - U_B)^2}{2\sigma(\rho_A + \rho_B)} - \frac{1}{2\sigma} \left[\frac{\rho_A^2\rho_B^2(U_A - U_B)^4}{(\rho_A + \rho_B)^2} - 4\sigma g(\rho_A - \rho_B) \right]^{1/2} \quad (29)$$

and

$$k_{\max}^c = \frac{\rho_A\rho_B(U_A - U_B)^2}{2\sigma(\rho_A + \rho_B)} + \frac{1}{2\sigma} \left[\frac{\rho_A^2\rho_B^2(U_A - U_B)^4}{(\rho_A + \rho_B)^2} - 4\sigma g(\rho_A - \rho_B) \right]^{1/2}. \quad (30)$$

On the other hand, given a particular density profile, the minimum velocity shear needed to destabilise the interface depends on the densities of the fluids and surface tension according to (Chandrasekhar 1961)

$$(U_A - U_B)_{\min}^2 = \frac{2(\rho_A + \rho_B)}{\rho_A\rho_B} [\sigma g(\rho_A - \rho_B)]^{1/2}. \quad (31)$$

2.4.2 Superfluid KH instability: a simple example

At first glance, the superfluid dispersion relation (24) has little in common with the classical dispersion relation (28). However, the underlying physics is similar, as can be seen by considering the special case $\rho_{s,A} = \rho_{s,B} = \rho_s$, $\rho_{n,A} = \rho_{n,B} = \rho_n$, $U_{s,A} = U_{n,A} = 0$, and $U_{s,B} = U_{n,B} = U$, which resembles a classical, single-fluid KH scenario. In this case, gravity cannot act as a stabilising force, because the densities of the top and bottom fluids are equal. However, there may easily exist another stabilising force which does not depend on the difference of densities (in Section 3.1.1, we discuss the possible origin of such a force). Thus we replace $g(\rho_{s,A} - \rho_{s,B})$ with F_s and $g(\rho_{n,A} - \rho_{n,B})$ with F_n . The dispersion relation now simplifies to

$$\begin{aligned} 0 = & (2\rho_s\omega^2 - 2\rho_s kU\omega + \rho_s k^2 U^2 - kF_s - k^3\sigma_s) \\ & \times \left[-\frac{2kF_n}{\rho_n} - \frac{2k^3\sigma_n}{\rho_n} + (2+r+\frac{1}{r})\omega^2 - 2(1+r)kU\omega + (1+r)k^2 U^2 \right] \\ & + (2\rho_n\omega^2 - 2\rho_n kU\omega + \rho_n k^2 U^2 - kF_n - k^3\sigma_n) \\ & \times \left[-\frac{2kF_s}{\rho_s} - \frac{2k^3\sigma_s}{\rho_s} + (2+r+\frac{1}{r})\omega^2 - 2(1+r)kU\omega + (1+r)k^2 U^2 \right], \end{aligned} \quad (32)$$

where $r = s_A/s_B$ is the entropy ratio. We can simplify this further by investigating the limit where the entropy of the bottom fluid is much greater than that of the top fluid, i.e. $r \rightarrow \infty$. Our dispersion relation then becomes

$$0 = [(2\rho_s\omega^2 - 2\rho_s kU\omega + \rho_s k^2 U^2 - kF_s - k^3\sigma_s) + (2\rho_n\omega^2 - 2\rho_n kU\omega + \rho_n k^2 U^2 - kF_n - k^3\sigma_n)](\omega - kU)^2, \quad (33)$$

whose roots can be found from $(\omega - kU)^2 = 0$, which represents a stable mode, and from

$$0 = 2(\rho_s + \rho_n)\omega^2 - 2(\rho_s + \rho_n)kU\omega + (\rho_s + \rho_n)k^2 U^2 - k(F_s + F_n) - k^3(\sigma_s + \sigma_n), \quad (34)$$

which represents an unstable mode if

$$k[2(\sigma_s + \sigma_n)k^2 - (\rho_s + \rho_n)U^2 k + 2(F_s + F_n)] < 0. \quad (35)$$

Therefore, the mode becomes unstable when U exceeds

$$U_{\min} = \left[\frac{16(\sigma_s + \sigma_n)(F_s + F_n)}{(\rho_s + \rho_n)^2} \right]^{1/4}. \quad (36)$$

Equation (36) reduces to the classical result $U_{\min}^c = (16F\sigma/\rho^2)^{1/4}$ for $\rho_A = \rho_B$ and is similar in form even for $\rho_A \neq \rho_B$. Therefore, the underlying physics of the classical and superfluid KH instabilities are similar, except that, in the latter scenario, the fluids consist of coupled normal and superfluid components, only the normal fluid can transport entropy, and the top and bottom superfluids contain different types of Cooper pairs and hence have different entropies even at the same temperature. The entropy difference shifts the critical density and shear velocity as discussed below and in Figs. 1 and 2. Interestingly, we expect $r \sim 1$ under a wide range of physical conditions, yet in this regime (32) does not factorize simply into (33). To recover the classical-like threshold (36), one needs $r \gg 1$, which is uncommon in nature.

2.4.3 Superfluid KH instability: general threshold

In the superfluid KH instability, the entropy ratio $r = s_A/s_B$ shifts the instability threshold. In Fig. 1, we plot the critical (minimum) density ratio $p = \rho_B/\rho_A$ as r changes for three different values of surface tension $\sigma/(\rho_A U_A^4 g^{-1}) = 0.22, 1.1,$ and 17.7 , while the top fluid is initially stationary. If $p < p_{\min}$, the interface is stable. In Fig. 2, we plot the critical (minimum) U as r changes, for $p = 0.1, 0.5,$ and 0.8 . If $U < U_{\min}$, the interface is stable. Tables 1 and 2 summarise the parameters used to construct these figures. From Figs. 1 and 2, we see that the shift of the instability threshold away from classical expectations increases as $|s_A - s_B|$ increases. Moreover, as $|s_A - s_B|$ increases, the interface becomes unstable more easily; interfacial waves are induced for a wider range of k , and stability no longer depends solely on density ratio or velocity shear. Classically, the KH instability is driven by a difference in velocity, which causes a difference in pressure between the top and bottom layers of the interface by Bernoulli's law. In a superfluid, the temperature gradient $\nabla\tau$ is also a driving force (or, more generally, the gradient in chemical potential). Thus, a differential shear flow at the interface drives a temperature difference between the layers through (3), destabilising the interface. The magnitude of this effect is related to s_A/s_B , since in the momentum equations (1) and (2) the temperature gradient force is proportional to entropy.

In our analysis, we ignore the effects of the container wall. This is justified in the case of the free 1S_0 - 3P_2 interface in a neutron star. The friction between the fluids and the container wall also lowers the instability threshold, as concluded by Volovik (2002).

3 CIRCULATION TRANSFER

In this section, we calculate the wavelength and growth rate of the KH instability for the terrestrial Blaauwgeers et al. (2003) experiment and neutron star crust-core interface. In both cases, we also calculate the circulation transferred across the interface, which is proportional to the number of vortex lines per KH wavelength.

The parameters pertaining to the terrestrial experiment (Blaauwgeers et al. 2003) are summarised in Table 3. The superfluid density is drawn from the table of total fluid densities given by Putterman (1974), assuming normal fluid densities between $10^{-3}\rho_s$ and $10^{-1}\rho_s$ (the superfluid component dominated in the experiment). The surface tension at the interface is extrapolated from the experimental results of Osheroff & Cross (1977) and Bartkowiak et al. (2004), the latter for small apertures, which range from 3×10^{-9} to 6×10^{-9} N m $^{-1}$. Taking $\sigma = 10^{-8}$ N m $^{-1}$ and applying eq. (2) from Blaauwgeers et al. (2003), we extrapolate the stabilising magnetic force density to be 5 N m $^{-3}$.

The parameters pertaining to the neutron star crust-core interface are summarised in Table 4. Four cases are considered. In Case A, we investigate the instability at the crust-core interface of a typical neutron star, with density and shear velocity profile taken from Tsuruta (1979), Nomoto & Tsuruta (1987), Yakovlev, Levenfish & Shibano (1999), Tsuruta (1998), and Svidzinsky (2003). The surface tension is extrapolated from Osheroff & Cross (1977), Bartkowiak et al. (2004), and Privorotskii (1975). In Cases B, C, and D, we investigate how the instability behaves as we vary the density ratio p for $r = 0.1, 1,$ and 10 .

3.1 Blaauwgeers et al. (2003) experiment

3.1.1 Experimental parameters

In this laboratory experiment, He-A and He-B were superposed in differential rotation. The interface between He-A and He-B was magnetically stabilised and the container rotated, inducing rotation in the normal fluid on both sides of the interface, which then drags the superfluid component of the A-phase into rotation. The superfluid component of the B-phase was initially stationary. Above a critical rotational speed, the B-phase superfluid experienced sudden jumps in rotation speed, measured as jumps in the B-phase nuclear magnetic resonance absorption signal. This was interpreted as the transfer of vortex lines from the A-phase into the B-phase across the destabilized interface (Blaauwgeers et al. 2003).

The experiment was conducted at $T = 0.77T_c$, $p = 29$ bar. The A-phase normal and superfluid components as well as the B-phase normal fluid rotated together at 0.0039 m s $^{-1}$, while the B-phase superfluid was initially stationary. The value we adopt for the superfluid density, $\rho_s = 100$ kg m $^{-3}$, is taken from the table of total fluid densities given in Putterman (1974). The normal fluid density is lower but an exact figure is not quoted; we try $\rho_n = 0.1, 1.0,$ and 10 kg m $^{-3}$ (labelled as Case 1,

2, and 3 respectively). At the superfluid A-B interface, the order parameter of the BCS pair fluid (analogous to magnetisation in a ferromagnet) changes abruptly, causing surface tension (Osheroff & Cross 1977; Bartkowiak et al. 2004). At $T = 0.77T_c$ and $p = 29$ bar, experiments measure $0.3 \leq \sigma_s / (10^{-8} \text{ N m}^{-1}) \leq 0.6$; we adopt $\sigma_s = 10^{-8} \text{ N m}^{-1}$ for simplicity. The magnetic restoring force density produced by the magnetic susceptibility gradient across the interface, $F = (1/2)(\chi_A - \chi_B)\nabla(H_b^2) \approx 5 \text{ N m}^{-3}$, where χ_A and χ_B are the susceptibilities of the A- and B-phase respectively and H_b is the magnetic field applied, is estimated by substituting σ_s into the approximate formula put forward by Blaauwgeers et al. (2003) (on the last page of that paper) to explain the observed number of vortex lines transferred across the interface.

Gravity cannot act as the restoring force, because the top and bottom fluids are of the same densities, so the dispersion relation (24) needs to be modified to replace gravity with the magnetic force, viz.

$$0 = [\rho_{s,B}^0(-\omega + k_x U_{s,B})^2 + \rho_{s,A}^0(-\omega + k_x U_{s,A})^2 - k^3 \sigma_s - k F_s] \left[-\frac{k}{2}(\rho_{s,A}^0 + \rho_{s,B}^0) F_n - \frac{k^3}{2}(\rho_{s,A}^0 + \rho_{s,B}^0) \sigma_n + \alpha \gamma \right] \\ + [\rho_{n,B}^0(-\omega + k_x U_{n,B})^2 + \rho_{n,A}^0(-\omega + k_x U_{n,A})^2 - k^3 \sigma_n - k F_n] \left[-\frac{k}{2}(\rho_{n,A}^0 + \rho_{n,B}^0) F_s - \frac{k^3}{2}(\rho_{n,A}^0 + \rho_{n,B}^0) \sigma_s + \alpha \beta \right]. \quad (37)$$

Our model treats the superfluid and normal fluid components equivalently; we are free to put the surface tension and magnetic restoring force into σ_s and F_s or σ_n and F_n . In reality, of course, there is only one surface tension and one magnetic restoring force, as experiments cannot distinguish between superfluid and normal fluid interfaces. However, according to the interpretation of the experiment tendered by Blaauwgeers et al. (2003), the A-phase and B-phase normal fluids move together as one continuous fluid, so we set $\sigma_n = 0$, $F_n = 0$, $\sigma_s = 10^{-8} \text{ N m}^{-1}$, and $F_s = 5 \text{ N m}^{-3}$ in the absence of more detailed measurements. We note that the results are insensitive to this choice: setting $F_n = F_s = 5 \text{ N m}^{-3}$ shifts k_{\min} by 0.07 per cent for Case 1, 0.6 per cent for Case 2, and 9 per cent for Case 3.

3.1.2 Instability threshold and growth rate

In the Blaauwgeers et al. (2003) experiment, the normal fluid components are comoving, so the normal fluid interface is absolutely stable. Nevertheless, just by being there, the normal fluid significantly affects the instability threshold due to its ability to transport entropy via (3). This is an important result. We plot the threshold wavenumber k_{\min} versus the entropy ratio r in Fig. 3. In all three cases (labelled Case 1, 2, and 3), the interface becomes unstable at k_{\min} different from the classical value (which is $7.3 \times 10^3 \text{ m}^{-1}$), particularly at lower r , where k_{\min} is much less than the classical value.² We see that k_{\min} increases with r , jumps sharply at $\log r \approx -0.6$, then decreases gently; we find $1.0 \leq k_{\min}/k_{\min}^C \leq 1.1$ between $-0.1 \leq \log r \leq 0.1$. The jump occurs at a slightly lower r in Case 3, where ρ_n is smaller than in Cases 1 and 2. At low r , the k_{\min} is lowest (i.e. the interface is least stable) when ρ_n is highest (Case 3), indicating that the presence of more normal fluid (whose interface is KH stable by assumption) helps destabilise the superfluid interface. However, this trend shifts at $\log r \geq 0.65$, where more normal fluid density helps stabilise the interface. Interestingly, the superfluid interface is stable classically for, say, $F_s \geq 60 \text{ N m}^{-3}$ but not when entropic effects are included, when it is unstable for $\log r \leq -0.6$ and $\log r \geq 1.6$.

Classically, the normal fluid is not expected to influence the stability of the superfluid interface (in this experiment, where the normal fluid interface is absolutely stable, the normal fluid seems naively to act as a passive background). Yet our analysis shows that it does affect the stability significantly, indicating that it is driven not only by the shear flow, but also by a ‘drag effect’ (Blaauwgeers et al. 2003) between the superfluid and normal fluid components in the B-phase, the strength of which depends on the relative amounts of normal fluid and superfluid present. This effect comes from the term proportional to v_{ns} in (1) and (2).

In Fig. 4, we plot the growth rate of the instability [the maximum of $\text{Im}(\omega)$] for the three cases above. From Fig. 4, for $r \sim 1$, we obtain a growth time ~ 22 ms, close to the classical value. This maximum value for $\text{Im}(\omega)$ is associated with cutoff wavenumber $k_{\text{cutoff}} = 4.71 \times 10^4$, 4.70×10^4 , and $4.45 \times 10^4 \text{ m}^{-1}$ for Cases 1, 2, and 3 respectively. Note that $k_{\text{cutoff}} \sim 6k_{\min}$. The instability in Case 3, where ρ_n is highest, grows most quickly, indicating that the superfluid interface is destabilised even further by the normal fluid, through the drag effect. We anticipate that our prediction of the KH growth time will be tested by future nuclear magnetic resonance measurements.

² The classical value needs careful interpretation in this situation, because the Blaauwgeers et al. (2003) experiment differs slightly from standard KH instability scenarios. The superfluid-superfluid interface resembles the classical KH setup, with the top fluid moving and the bottom stationary, but the normal fluid components are comoving, so the normal fluid interface is absolutely stable. Consequently, setting $\alpha = 0$ in (24) does not lead to the correct classical (nonentropic) limit. Instead, one should ignore the normal fluid completely and apply the classical formula to the superfluid-superfluid interface (Blaauwgeers et al. 2003).

3.1.3 Angular velocity jump

When the interface becomes unstable, it is hypothesised that superfluid vortex lines break through the interface and transfer circulation from one fluid to the other. As circulation is quantized, the amount transferred depends on the wavelength of the KH instability, that is, on how many vortex lines (δN) can fit within one corrugation of the wave. A-phase vortex lines are $\sim 10^3$ times thicker radially than B-phase ones, so a concentration of energy is needed to push and convert A-phase lines into B-phase lines. This free energy is provided by the instability at the interface (Blaauwgeers et al. 2003). The precise mechanism of vortex transfer and conversion is still unknown, but Volovik (2002) suggested that the vortices in the A-phase are pushed by the Magnus force towards the vortex-free B-phase, entering the potential well formed by the corrugation of the unstable interface and enhancing the growth of the well until it forms a droplet of A-phase fluid filled with vorticity, which then resides in the B-phase (Volovik 2002).

For Cases 1, 2, and 3, k_{\min} at $r \approx 1$ is approximately equal to the classical value of 7300 m^{-1} , giving an instability wavelength $\lambda_0 = 2\pi/k_{\min} = 8.6 \times 10^{-4} \text{ m}$. The amount of circulation transferred across the interface is $\kappa = |U_A - U_B|\lambda_0/2$ (Volovik 2002). The circulation quantum of superfluid ${}^3\text{He}$ is $\kappa_0 = h/2m_3 = 6.6 \times 10^{-8} \text{ m}^2 \text{ s}^{-1}$, where m_3 is the mass of a ${}^3\text{He}$ atom. Our analysis of the Blaauwgeers et al. (2003) experiment thus implies $\kappa = 1.7 \times 10^{-6} \text{ m}^2 \text{ s}^{-1}$ and $\delta N = \kappa/\kappa_0 \approx 25$. Experimentally, Blaauwgeers et al. (2003) observed $\delta N \approx 10$. The discrepancy may be due, in part, to misestimating of $\sigma_{n,s}$, $F_{n,s}$, and/or $\rho_{n,s}$ in the absence of exact quoted values. We take heart, however, from semiquantitative agreement between theory and experiment and proceed to apply the theory to the crust-core interface in a neutron star.

3.2 Neutron star 1S_0 - 3P_2 interface

3.2.1 Stellar parameters

We assume that the phase transition from 1S_0 to 3P_2 neutron superfluid in a neutron star occurs at a sharp boundary near the crust-core interface at radius $R \approx 6 \text{ km}$ (Yakovlev, Levenfish & Shibano 1999). The inner crust consists entirely of neutron BCS pairs in the 1S_0 state, behaving as an isotropic superfluid of density $\rho_B = 1.5 \times 10^{17} \text{ kg m}^{-3}$ (Tsuruta 1979; Nomoto & Tsuruta 1987; Yakovlev, Levenfish & Shibano 1999; Svidzinsky 2003). The temperature of the crust is around 10^8 K , which is about $0.01T_c$ (Tsuruta 1998; Yakovlev, Levenfish & Shibano 1999) so the normal fluid is negligible; we therefore assume $\rho_s = 1.5 \times 10^{17} \text{ kg m}^{-3}$ and $\rho_n = 1.5 \times 10^{15} \text{ kg m}^{-3}$ in the absence of detailed knowledge. The core consists of neutron BCS pairs in the 3P_2 state, with $T = 0.2T_c = 10^8 \text{ K}$ (Yakovlev, Levenfish & Shibano 1999). Hence the superfluid component is dominant here also; we assume $\rho_s = 2.8 \times 10^{17} \text{ kg m}^{-3}$ and $\rho_n = 2.8 \times 10^{15} \text{ kg m}^{-3}$. This density and shear velocity profile we label as Case A, summarised in Table 4. We also calculate how the instability wave number k_{\min} changes with respect to density ratio $p = \rho_{\text{crust}}/\rho_{\text{core}}$ with density ratio r fixed at 0.1, 1, and 10. We present these results as Cases B, C, and D respectively in Table 4. Note that, in the subsonic regime we investigate, the neutron star matter is approximately incompressible.

The surface tension at the neutron star crust-core interface is unknown. However, according to Privorotskii (1975), surface tension scales as $m^* p_F T_c^2 (1 - T/T_c)^{3/2}$, where m^* is the effective mass of the particles and p_F is the Fermi momentum. Noting that p_F in a neutron superfluid is $\sim 2 \times 10^5$ times higher than terrestrial ${}^3\text{He}$ and T_c is $\sim 10^{11}$ times higher, and terrestrial ${}^3\text{He}$ is measured to have $\sigma_s = 10^{-8} \text{ N m}^{-1}$ (Osheroff & Cross 1977; Bartkowiak et al. 2004), we estimate that the surface tension of neutron star superfluid is $\sigma_s \sim 10^{19} \text{ N m}^{-1}$, i.e. 25 orders of magnitude higher proportionately. We are acutely aware of the shortcomings of this estimate and hope that more reliable calculations will be undertaken in the literature in the future.

3.2.2 Glitch threshold and growth rate

We plot k_{\min}/k_{\min}^C versus $\log r$ for Case A in Fig. 5, where $k_{\min}^C \approx 0.67 \text{ m}^{-1}$ is the classical value of the instability threshold, obtained by setting $\alpha = 0$ in (24). We see that as r increases, the interface becomes less stable. The instability wave number k_{\min} is inversely proportional to shear velocity U and directly proportional to gravitational acceleration g , as purely classical KH instability theory predicts (Chandrasekhar 1961). At low r , the plot is flat and k_{\min} is fairly close to the classical value ($k_{\min} = 2.662, 0.666, \text{ and } 0.167 \text{ m}^{-1}$ for $U = 5 \times 10^5, 10^6, \text{ and } 2 \times 10^6 \text{ m s}^{-1}$ respectively). Case A is classically unstable, but the shift in k_{\min} is only noticeable at higher r , where the plot dips at $\log r \geq -0.5$. Note that we find $k_{\min} R_* \gg 1$, so the assumption of a plane wave perturbation is justified *a posteriori*.

One can also vary the density ratio p while keeping r constant. In Fig. 6, we plot k_{\min} against p for three different

³ We attempted to calculate the exact temperature-dependent value of ρ_n/ρ_s from eqs. (3.92) and (3.94) in Vollhardt & Wölfle (2002). However, due to uncertainties in m^* and the Fermi-liquid corrections in a neutron superfluid, we obtained $\rho_n \approx 0.3\rho_{\text{total}}$ at $T = 0.01 T_c$, which seems to be higher than existing phenomenological models can sustain (Link, Epstein & Baym 1993). Thus we take $\rho_n = 0.01\rho_{\text{total}}$ for now.

entropy ratios $r = 0.1, 1,$ and $10,$ labelled as Cases B, C, and D respectively (see Table 4). The classical minimum wave number approaches infinity as the top fluid density reaches zero, i.e. the interface becomes absolutely stable as the top fluid disappears. When entropy is taken into account, k_{\min} still increases as p gets lower, but at a slower rate, especially at higher $r.$ Cases B, C, and D join the classical curve at $p \approx 0.45, 0.9,$ and $1.0,$ demonstrating again that we diverge further from the classical expectation as $|s_A - s_B|$ increases.

In the foregoing, we do not consider the effects of a magnetic field and susceptibility discontinuity at the interface. In principle, a magnetic field can stabilise the boundary as in the Blaauwgeers experiment (see Section 3.1). We can set an approximate upper bound on $\nabla(H_b^2)$ at $B^2/(\mu_0^2 R),$ where B is the magnetic field at the surface of the star (typically $10^8 - 10^9$ T). Thus, the upper bound on the magnetic force density is between 1.06×10^{24} and 1.06×10^{26} N m $^{-3}.$ However, we find that, for Case A (i.e. typical neutron star parameters), the minimum magnetic force density necessary to stabilise the interface occupies the range $2.4\text{--}2.9 \times 10^{38}$ N m $^{-3}$ for $-2 \leq \log r \leq 1,$ much higher than the maximum force density available.

For a given shear velocity and density profile, one can now estimate the growth rate γ of the instability. We present our plot of growth rate versus r for a standard neutron star density profile (Case A) as Fig. 7; the classical growth rate is $\text{Im}(\omega^c) = 1.77 \times 10^{15}$ s $^{-1}$ for these parameters. The growth rate is found to be directly proportional to the cube of the shear velocity and inversely proportional to surface tension. We find $\gamma \approx 1.01\gamma^c$ for $r \sim 1.$ The growth time grows monotonically with k and takes the value of 5.59×10^{-16} s at $k_{\text{cutoff}} = 6.53 \times 10^9$ m $^{-1}$ (where k_{cutoff} is determined by the surface tension).

If there is no surface tension, the viscosity of the fluid suppresses the KH instability when the viscous time-scale is shorter than the growth time of the KH oscillation, i.e. for $k^2\nu^{-1}\text{Im}(\omega),$ where ν is the kinematic viscosity. The viscosity of superfluid neutron star matter is estimated to lie between 0.1 and 0.17 m 2 s $^{-1}$ for Case A (Andersson, Comer & Glampedakis 2004). In Fig. 8, we present a plot of $\text{Im}(\omega)$ versus $r.$ We find $\text{Im}(\omega) \propto U^2\nu^{-1}.$ For Case A, if the surface tension vanishes but viscosity suppresses the instability, we estimate $\text{Im}(\omega) = 1.1\text{Im}(\omega^c)$ and $k_{\text{cutoff}} = 5.24 \times 10^6$ m $^{-1}$ for $r = 1,$ translating into a growth time of 4×10^{-13} s. The growth time is $\sim 10^3$ times larger than the limit imposed by surface tension above, indicating that viscosity suppresses the instability more effectively than surface tension.

Prima facie, our KH growth time estimate seems too small; certainly, it is unresolvable by radio pulsar timing. However, it is highly dependent on k_{cutoff} ($k_{\text{cutoff}} \gg k_{\min},$ unlike in the terrestrial experiment). As k_{cutoff} depends on dissipation physics which is largely neglected in our model, e.g. textural terms on the right-hand sides of (1) and (2), a more complete analysis is needed before the KH growth time can be predicted with confidence.

3.2.3 Angular velocity jump

For typical neutron star parameters (Case A), near $r = 1,$ we obtain $k_{\min} \approx 0.587$ m $^{-1},$ and hence $\lambda_0 = 10.7$ m. This implies that the amount of circulation transferred across the interface is $\kappa = |U_A - U_B|\lambda_0/2 = 5.35 \times 10^6$ m 2 s $^{-1}.$ The total circulation at the interface is roughly $2\pi R|U_A - U_B| \approx 6 \times 10^9$ m 2 s $^{-1}.$ Therefore, the fractional change in angular velocity is $\Delta\Omega/\Omega \approx \lambda_0 R \approx 1.4 \times 10^{-4}.$ This compares surprisingly well with observations of the angular velocity jump in pulsar glitches, viz. $10^{-9} < \Delta\Omega/\Omega < 10^{-4}$ (Shemar & Lyne 1996).

3.2.4 Proton superfluid

Hydrodynamic models of neutron star superfluids in the literature (Mendell 1991; Andersson, Comer & Prix 2003) often include protons, electrons, and muons. The latter two species can be effectively incorporated into the normal fluid in our analysis (Mendell 1991), but the protons cannot. How significant is the proton superfluid?

One key effect of the protons is the drag they exert on the neutrons. The strength of the ‘drag effect’ between the protons and neutrons is set by the off-diagonal elements of the symmetrical mass density matrix, i.e. $\rho_{np} = \rho_{pn} = \rho_n(m_n^* - m_n)/m_n^* = \rho_p(m_p^* - m_p)/m_p^*,$ where ρ_n (ρ_p), m_n (m_p), and m_n^* (m_p^*) are the neutron (proton) density, bare mass, and effective mass respectively. Estimates of m_p^* vary between $0.3m_p$ and $0.7m_p,$ while ρ_p can be estimated from neutron star cooling rates (Tanigawa, Matsuzaki & Chiba 2004). If we take the proton density to be 15 per cent of the total core density of 2.8×10^{17} kg m $^{-3},$ the threshold proton fraction for direct URCA cooling (Tanigawa, Matsuzaki & Chiba 2004), we obtain $|\rho_{np}/\rho_n| \sim 0.15.$ Hence the proton-neutron drag force in Eq. (14) of Mendell (1991), as a fraction of a typical term in our momentum equation (1), is given by $(\rho_{np}/\rho)|\mathbf{v}^{(p)} - \mathbf{v}^{(n)}| |\nabla \times \mathbf{v}^{(n)}|/|\mathbf{v}^{(n)}|\omega \lesssim (\rho_{np}/\rho)(2kv^{(n)}/\omega) \sim 0.3$ (for a typical KH instability, the phase velocity is of the same order as the shear velocity), where $\mathbf{v}^{(n)}$ ($\mathbf{v}^{(p)}$) is the neutron (proton) superfluid velocity. In other words, the proton-neutron drag is smaller than, but comparable to, the forces we consider and should be included in general. It is omitted in this paper to keep the algebra manageable and to maintain focus on the entropic KH effects, presented here for the first time. Note that, although the normal fluid fraction under neutron star conditions may be low, the entropy ratio r is what matters in our analysis, and it is not negligible.

There are other physical effects that also appear when charged species are included. In this paper, we intentionally neglect electromagnetic forces [see Eqs. (15) and (16) in Mendell (1991)] and electromagnetic contributions to the chemical potential [Eqs. (29) and (30) in Mendell (1991)], again to render the superfluid KH analysis tractable. One electromagnetic effect is

included: the force term $F_{n,s}$, which can stabilise the interface in principle (see Section 3.1.1 above), although in practice it is too weak to shift k_{\min} appreciably in a neutron star (see Section 3.2.2). Apart from excluding the proton superfluid, our hydrodynamic equations are similar to those written down by Mendell (1991). In our case, the coupling is between the normal fluid and superfluid components and is governed by entropy (this coupling has been unambiguously observed in laboratory experiments, e.g. second sound in He II). Our terms involving entropy and counterflow are derived from the gradient of the chemical potential (see Section 2.1) and therefore are implicitly included in the neutron superfluid chemical potential $\tilde{\mu}_n$ [Eq. (29) in Mendell (1991)]. Another important difference is that Mendell (1991) and Andersson, Comer & Prix (2003) deal with a non-stratified neutron star which consists of two different but interpenetrating superfluids, whereas we deal with a stratified (two-zone) neutron star with two layers of superfluid in differential rotation.

4 CONCLUSIONS

We analyse the superfluid KH instability within the framework of two-fluid hydrodynamics including entropy flow and both the superfluid and normal fluid components in each fluid. We find that the coupling between the superfluid and the normal fluid components via entropy transport lowers the instability threshold (especially when the entropy ratio is large) even if there is no significant counterflow. When the counterflow is significant, as in the experiment conducted by Blaauwgeers et al. (2003), the reduction in the threshold is even greater. Classically, the KH instability occurs because the velocity shear induces a self-reinforcing pressure gradient across the interface. In a superfluid, the (perturbed) temperature gradient, driven by the differential flow, is also a driving force, the magnitude of which is controlled by ratio of the entropies of the fluids, and the interface becomes less stable than expected classically.

When the interface crinkles, it is believed that superfluid vortex lines break through and transfer circulation between the fluids, although the mechanism is not understood at the Gross-Pitaevskii level. Since circulation is quantized, the amount transferred depends on how many vortex lines can fit in one corrugation of the KH surface wave. Applied to Blaauwgeers et al. (2003) experiment, our model yields a growth time of ~ 22 ms and threshold wavenumber $k_{\min} = 7.3 \times 10^3 \text{ m}^{-1}$, so that the number of vortex lines transferred is $\delta N \approx 25$. The observed number of vortex lines is 10 (Blaauwgeers et al. 2003). Applied to the neutron star crust-core (1S_0 - 3P_2) interface, with $U = 10^6 \text{ m sec}^{-1}$ and $r = 1$, we find $\lambda_0 = 11 \text{ m}$, so that the fractional change in angular velocity is $\Delta\Omega/\Omega \approx \lambda_0 R \approx 1.4 \times 10^{-4}$. This compares favourably with typical pulsar glitch events, which are observed to have $10^{-9} < \Delta\Omega/\Omega < 10^{-4}$ (Shemar & Lyne 1996). In view of this estimate, and the high KH growth rate, it is possible that vortex line transfer through a surface KH instability may explain pulsar glitches. An alternative process, the two-stream instability of isotropic neutron and proton superfluids in differential rotation, is also an attractive possibility (Andersson, Comer & Prix 2003). A more thorough analysis of both, taking into account the nonuniform texture and anisotropic densities and thermal conductivities of the core superfluid, is worth pursuing.

ACKNOWLEDGMENTS

We thank Derek Chan, Barry Hughes, James McCaw, Bruce McKellar, Andy Martin, Thanu Padmanabhan, and Chris Pakes for discussions.

REFERENCES

- Andersson N., Comer G.L., Glampedakis K., 2004, preprint(astro-ph/0411748)
 Andersson N., Comer G.L., Prix R., 2003, Phys. Rev. Lett., 90, 091101
 Barenghi C., Jones M., 1988, Journal of Fluid Mech., 197, 551
 Bartkowiak M., Fisher S.N., Guénault A.M., Haley R.P., Pickett G.R., Skyba P., 2004, Phys. Rev. Lett., 93, 045301
 Baym G., Pethick C.J., 1975, Ann. Rev. Nucl. & Particle Phys., 1975, 27
 Blaauwgeers R., Eltsov V.B., Eska G., Finne A.P., Haley R.P., Krusius M., Ruohio J.J., Skrbek L., Volovik G.E., 2002, Phys. Rev. Lett., 89, 155301
 Brand H., Pleiner H., 1981, Phys. Rev. D, 24, 3048
 Chandrasekhar S., 1961, Hydrodynamic and Hydromagnetic Stability. Dover Publications Inc., New York
 Flowers E., Ruderman M., Sutherland P., 1976, ApJ, 205, 541
 Hall H.E., Vinen W.F., 1956, Proc. Roy. Soc. Lond. A, 238, 215
 Hoffberg M., Glassgold A.E., Richardson R.W., Ruderman M., 1970, Phys. Rev. Lett., 24, 775
 Jones P.B., 1998, MNRAS, 296, 217
 Khalatnikov I.M., 2000, An Introduction to the Theory of Superfluidity. Perseus Publishing, Cambridge
 Khodel V.V., Khodel V.V., Clark J.W., 2001, Nucl. Phys. A, 679, 827

Table 1. Fluid parameters for the calculation of threshold density ratio $p = \rho_B/\rho_A$ as a function of entropy ratio $r = s_A/s_B$ in Fig. 1. The top fluid B is stationary. The superfluid and normal fluid components of the bottom fluid A move at the same velocity U_A . We investigate three values of U_A (Cases I–III). The classical thresholds are $p_{\min}^c = 0.997, 0.947,$ and 0.780 for Cases I–III respectively.

Parameters	Case I	Case II	Case III
$\rho_{n,A}/\rho_A$	9.90×10^{-3}	9.90×10^{-3}	9.90×10^{-3}
$\rho_{s,A}/\rho_A$	9.90×10^{-1}	9.90×10^{-1}	9.90×10^{-1}
U_B/U_A	0	0	0
$\sigma_n [g^{-1} \rho_A U_A^4]^{-1}$	17.7	1.10	2.18×10^{-1}
$\sigma_s [g^{-1} \rho_A U_A^4]^{-1}$	17.7	1.10	2.18×10^{-1}

Table 2. Fluid parameters for the calculation of threshold velocity shear U_{\min} as a function of entropy ratio $r = s_A/s_B$ in Fig. 1. The top fluid B is stationary. The superfluid and normal fluid components of the bottom fluid A move at the same velocity U_{\min} . We investigate three values of $p = 0.1, 0.5,$ and 0.8 (Cases IV–VI).

Parameters	Case IV	Case V	Case VI
$\rho_{n,B}/\rho_A$	9.90×10^{-4}	4.95×10^{-3}	7.92×10^{-3}
$\rho_{s,B}/\rho_A$	9.90×10^{-2}	4.95×10^{-1}	7.92×10^{-1}
$\rho_{n,A}/\rho_A$	9.90×10^{-3}	9.90×10^{-3}	9.90×10^{-3}
$\rho_{s,A}/\rho_A$	9.90×10^{-1}	9.90×10^{-1}	9.90×10^{-1}
$\sigma_n [g^{-1} \rho_A (U_{\min}^c)^4]^{-1}$	2.29×10^{-3}	5.56×10^{-2}	2.47×10^{-1}
$\sigma_s [g^{-1} \rho_A (U_{\min}^c)^4]^{-1}$	2.29×10^{-3}	5.56×10^{-2}	2.47×10^{-1}
$U_{n,B}/U_{\min}^c$	0	0	0
$U_{s,B}/U_{\min}^c$	0	0	0

- Korshunov S.E., 2002, JETP Letters, 75, 423
Landau L.D., 1941, J. Phys., V, 71
Landau L.D., Lifshitz E.M., 1987, Fluid Mechanics, 2nd ed. Pergamon Press, Oxford
Lee D.M., 1997, Rev. Mod. Phys., 69, 645
Leggett A.J., 1975, Rev. Mod. Phys., 47, 331
Link B., Epstein R.I, Baym G., 1993, ApJ, 403, 285
Mendell G., 1991, ApJ, 380, 515
Nomoto K., Tsuruta S., 1987, ApJ, 312, 711
Osheroff D.D., Cross M.C., 1977, Phys. Rev. Lett., 38, 905
Privorotskii I.A., 1975, Phys. Rev. B, 12, 4825
Putterman S.J., 1974, Superfluid Hydrodynamics. North-Holland Publishing Company, Amsterdam
Svidzinsky A.A., 2003, ApJ, 590, 386
Shemar S.L., Lyne A.G., 1996, MNRAS, 282, 677
Tamagaki R., 1970, Prog. Theo. Phys., 44, 905
Tang Y.H., Hahn I., Bozler H.M., Gould C.M., 1991, Phys. Rev. Lett., 67, 1775
Tanigawa T., Matsuzaki M., Chiba S., 2004, Phys. Rev. C, 70, 065801
Tilley D.R., Tilley J., 1994, Superfluidity and Superconductivity, 3rd ed. IOP Publishing, Bristol
Tsuruta S., 1979, Phys. Reports, 56, 237
Tsuruta S., 1998, Phys. Reports, 292, 1
Tsuruta S., Canuto V., Lodenquai J., Ruderman M., 1972, ApJ, 176, 739
Vollhardt D., Wölfle P., 2002, The Superfluid Phases of Helium 3. Taylor & Francis, London
Volovik G.E., 2002, JETP Letters, 75, 418
Wheatley J.C., 1975, Rev. Mod. Phys., 47, 415
Wölfle P., 1979, Rep. Prog. Phys., 42, 271 Ann. Rev. Astron. Astrophys., 42, 169
Yakovlev D.G., Levenfish K.P., Shibanov Yu.A., 1999, Phys.Usp., 169, 825

APPENDIX A: INTEGRATING OVER INTERFACIAL DISCONTINUITIES

In general, a composite function of the form $g(x)f'(x)$, where both $f(x)$ and $g(x)$ are discontinuous at an interface $x = 0$, cannot be integrated across the discontinuity. Essentially, this is because the integral $\int dx \delta(x)\theta(x)$, where $\delta(x)$ and $\theta(x)$

Table 3. Fluid parameters for the instability threshold calculations as a function of entropy ratio r in Figs. 3 and 4. The parameters are taken from the spin-up experiment of Blaauwgeers et al. (2003). The bottom and top fluids are labelled A and B respectively. We investigate three values of density ratio p (Cases 1–3).

Parameters	Units	Case 1	Case 2	Case 3
$\rho_{n,B}$	kg m ⁻³	0.1	1	10
$\rho_{s,B}$	kg m ⁻³	100	100	100
$\rho_{n,A}$	kg m ⁻³	0.1	1	10
$\rho_{s,A}$	kg m ⁻³	100	100	100
$U_{n,B}$	m s ⁻¹	3.9×10^{-3}	3.9×10^{-3}	3.9×10^{-3}
$U_{s,B}$	m s ⁻¹	3.9×10^{-3}	3.9×10^{-3}	3.9×10^{-3}
$U_{n,A}$	m s ⁻¹	3.9×10^{-3}	3.9×10^{-3}	3.9×10^{-3}
$U_{s,A}$	m s ⁻¹	0	0	0
σ_n^a	N m ⁻¹	0	0	0
σ_s	N m ⁻¹	1×10^{-8}	1×10^{-8}	1×10^{-8}
F_n^b	N m ⁻³	0	0	0
F_s	N m ⁻³	5	5	5
k_{\min}^c	m ⁻¹	7.3×10^3	7.3×10^3	7.3×10^3

^a Surface tensions are extrapolated from the experimental results of Osheroff & Cross (1977) and Bartkowiak et al. (2004).

^b Magnetic restoring force is inferred from Blaauwgeers et al. (2003) and the surface tension.

^c Classical minimum instability wavenumber.

Table 4. Fluid parameters for the instability threshold calculations as a function of entropy ratio r (Case A) and density ratio p (Cases B–D). The crust fluid (B) is initially stationary in all cases; the core (A). In Case A, we investigate how the threshold wavenumber k_{\min} changes with entropy ratio $r = s_A/s_B$. In Cases B, C, and D, we investigate how k_{\min} changes with density ratio $p = \rho_B/\rho_A$ for $r = 0.1, 1.0,$ and 10 while keeping the density and velocity of the core constant.

Parameters	Units	Case A	Case B	Case C	Case D
g	m s ⁻²	5×10^{11}	5×10^{11}	5×10^{11}	5×10^{11}
$\rho_{n,B}$	kg m ⁻³	1.5×10^{15}	$2.8 \times 10^{14} - 2.8 \times 10^{15}$	$2.8 \times 10^{14} - 2.8 \times 10^{15}$	$2.8 \times 10^{14} - 2.8 \times 10^{15}$
$\rho_{s,B}$	kg m ⁻³	1.5×10^{17}	$2.8 \times 10^{16} - 2.8 \times 10^{17}$	$2.8 \times 10^{16} - 2.8 \times 10^{17}$	$2.8 \times 10^{16} - 2.8 \times 10^{17}$
$\rho_{n,A}$	kg m ⁻³	2.8×10^{15}	2.8×10^{15}	2.8×10^{15}	2.8×10^{15}
$\rho_{s,A}$	kg m ⁻³	2.8×10^{17}	2.8×10^{17}	2.8×10^{17}	2.8×10^{17}
$U_{n,B}$	m s ⁻¹	0	0	0	0
$U_{s,B}$	m s ⁻¹	0	0	0	0
$U_{n,A}$	m s ⁻¹	10^6	10^6	10^6	10^6
$U_{s,A}$	m s ⁻¹	10^6	10^6	10^6	10^6
σ_n^a	N m ⁻¹	10^{19}	10^{19}	10^{19}	10^{19}
σ_s	N m ⁻¹	10^{19}	10^{19}	10^{19}	10^{19}
F_n	N m ⁻³	0	0	0	0
F_s	N m ⁻³	0	0	0	0
r	—	0.01–10	0.1	1	10

^a Surface tensions are extrapolated from Osheroff & Cross (1977), Bartkowiak et al. (2004), and the theory in Privorotskii (1975).

are the Dirac delta and Heaviside step functions respectively, is ill-defined. However, if one assumes that the discontinuous functions change smoothly over the *same* small length-scale ϵ within the infinitesimal interval $\epsilon \leq x \leq \epsilon$, with $\epsilon \rightarrow 0$, the integral can be regularized. For example, to integrate $g(x)f'(x)$, one writes $f = \frac{b-a}{2\epsilon}x + \frac{b+a}{2}$ and $g = \frac{d-c}{2\epsilon}x + \frac{d+c}{2}$, such that the functions take well-defined values at the endpoints $f(-\epsilon) = a$, $g(-\epsilon) = c$, $f(\epsilon) = b$, and $g(\epsilon) = d$, yielding

$$\lim_{\epsilon \rightarrow 0} \int_{-\epsilon}^{+\epsilon} dx g f' = \frac{(b-a)(d+c)}{2}. \quad (\text{A1})$$

Another combination one encounters in (20) and (21) involves four discontinuous functions, of the form $l(x)h(x)g(x)f'(x)$. One writes $f = \frac{b-a}{2\epsilon}x + \frac{b+a}{2}$, $g = \frac{d-c}{2\epsilon}x + \frac{d+c}{2}$, $h = \frac{\beta-\alpha}{2\epsilon}x + \frac{\beta+\alpha}{2}$, and $l = \frac{\delta-\gamma}{2\epsilon}x + \frac{\delta+\gamma}{2}$, yielding

$$\begin{aligned} & \lim_{\epsilon \rightarrow 0} \int_{-\epsilon}^{+\epsilon} dx l h g f' \\ &= \frac{1}{24}(b-a) [(\delta+\gamma)(\beta-\alpha)(d-c) + (\delta-\gamma)(\beta+\alpha)(d-c) + (\delta-\gamma)(\beta-\alpha)(d+c)] + \frac{1}{8}(b-a)(\delta+\gamma)(\beta+\alpha)(d+c). \end{aligned} \quad (\text{A2})$$

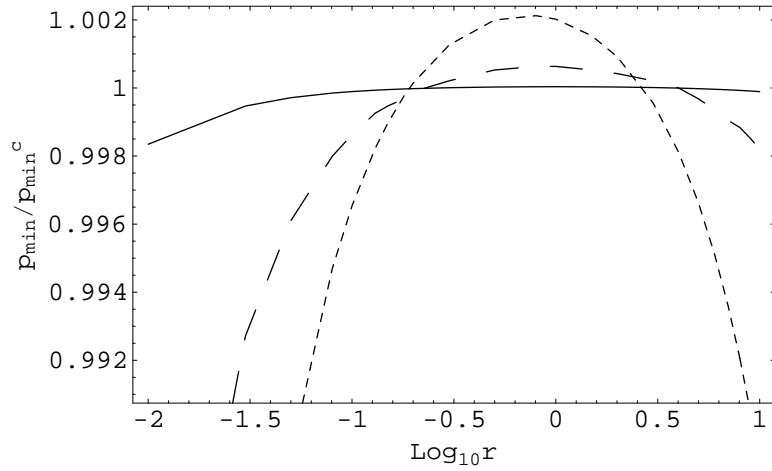


Figure 1. Instability threshold. Minimum density ratios p_{\min} (normalised to the classical value p_{\min}^c) plotted against $\log r$ for three different shear velocities, as in Table 1: Case I (solid curve, lowest U , $p_{\min}^c = 0.997$), Case II (dashed curve, intermediate U , $p_{\min}^c = 0.947$), and Case III (dotted curve, greatest U , $p_{\min}^c = 0.780$). The interface is stable if the system lies *below* the curves.

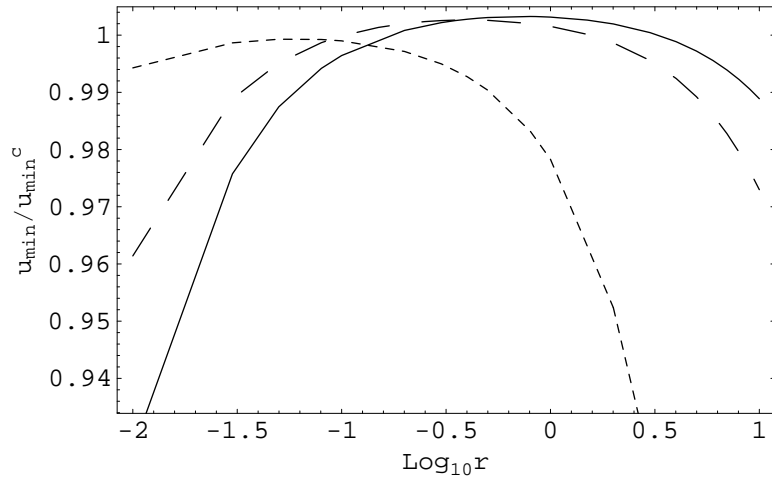


Figure 2. Instability threshold. Minimum shear velocity U_{\min} (normalised to the classical value U_{\min}^c) plotted against $\log r$ for three different density ratios p , as in Table 2: Case VI (solid curve, $p = 0.1$), Case V (dashed curve, $p = 0.5$), and Case IV (dotted curve, $p = 0.8$). The interface is stable if the system lies *below* the curves.

One can replace the linear trial functions above with other smooth trial functions, such as trigonometric functions; the results do not change. We emphasize again that there is no unique result for integrals of products of discontinuous functions of the kind above. For example, $\int dx g(x)f'(x)$ takes different values depending on the relative length-scales over which g and f change, which are determined physically. The results above pertain to the case where both g and f jump over an interval $O(\epsilon)$.

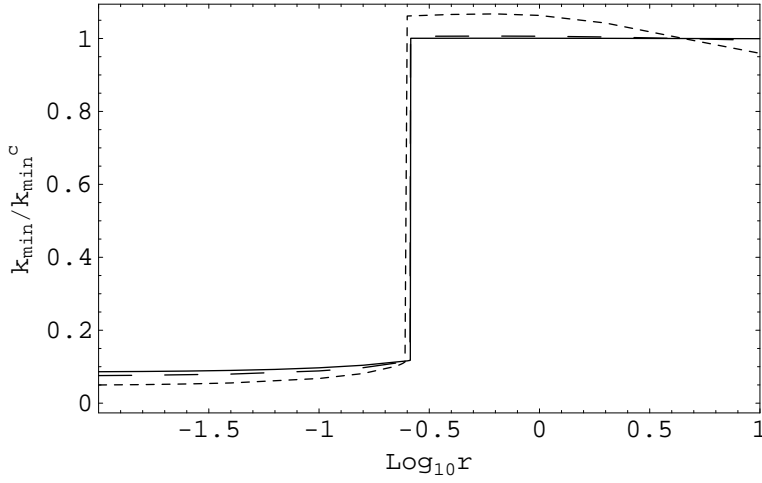


Figure 3. Threshold wavenumber k_{\min} versus entropy ratio r for the Blaauwgeers et al. (2003) experiment. The classical threshold wavenumber $k_{\min}^c = 7.3 \times 10^3 \text{ m}^{-1}$. The solid curve is Case 1 ($\rho_{n,A} = \rho_{n,B} = 0.1 \text{ kg m}^{-3}$), the dashed curve is Case 2 ($\rho_{n,A} = \rho_{n,B} = 1 \text{ kg m}^{-3}$), and the dotted curve is Case 3 ($\rho_{n,A} = \rho_{n,B} = 10 \text{ kg m}^{-3}$).

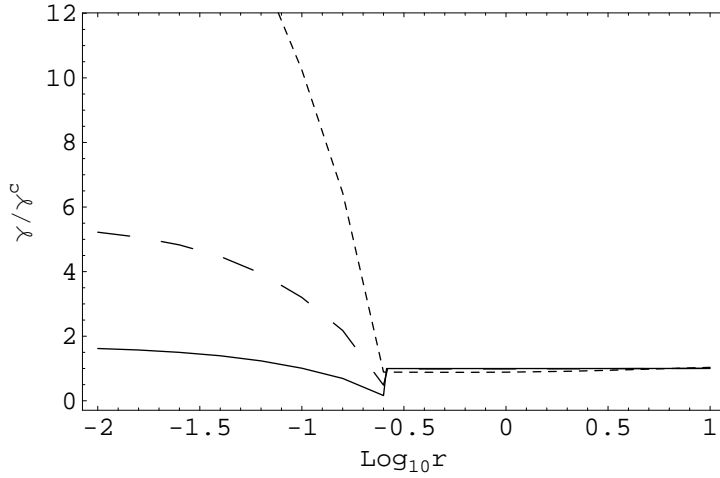


Figure 4. Maximum growth rate γ versus entropy ratio r for the Blaauwgeers et al. (2003) experiment, normalised to the classical growth rate $\gamma^c = 45.10 \text{ s}^{-1}$. The solid curve is Case 1 ($\rho_{n,A} = \rho_{n,B} = 0.1 \text{ kg m}^{-3}$), the dashed curve is Case 2 ($\rho_{n,A} = \rho_{n,B} = 1 \text{ kg m}^{-3}$), and the dotted curve is Case 3 ($\rho_{n,A} = \rho_{n,B} = 10 \text{ kg m}^{-3}$).

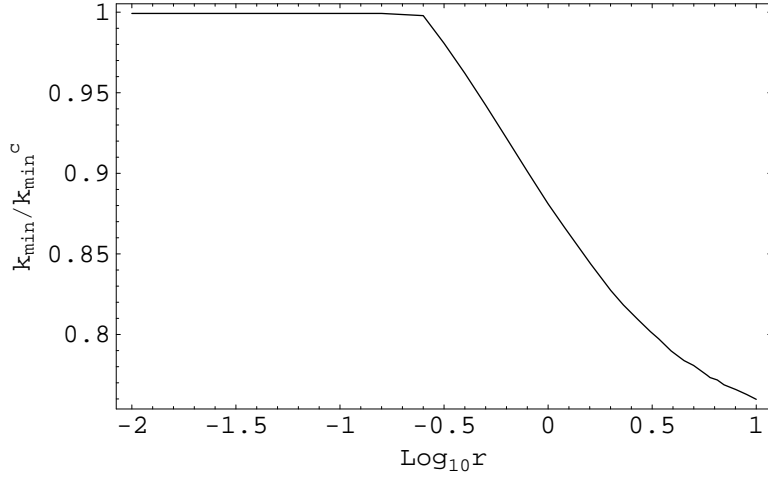


Figure 5. Threshold wavenumber k_{\min} versus entropy ratio r at the crust-core boundary of a standard neutron star. This is labelled as Case A ($U_{\text{core}} = 10^6 \text{ m s}^{-1}$) is Table 4. The classical threshold wavenumber $k_{\min}^c = 0.67 \text{ m}^{-1}$. We find that $k_{\min} \propto gU^{-2}$.

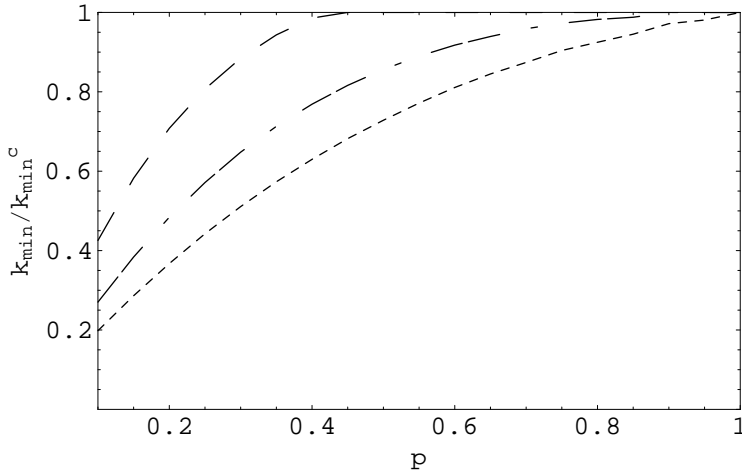


Figure 6. Threshold wavenumber k_{\min} versus density ratio p at the crust-core boundary of a neutron star. The dashed curve is Case B ($r = 0.1$), the dashed-dotted curve is Case C ($r = 1$), and the dotted curve is Case D ($r = 10$).

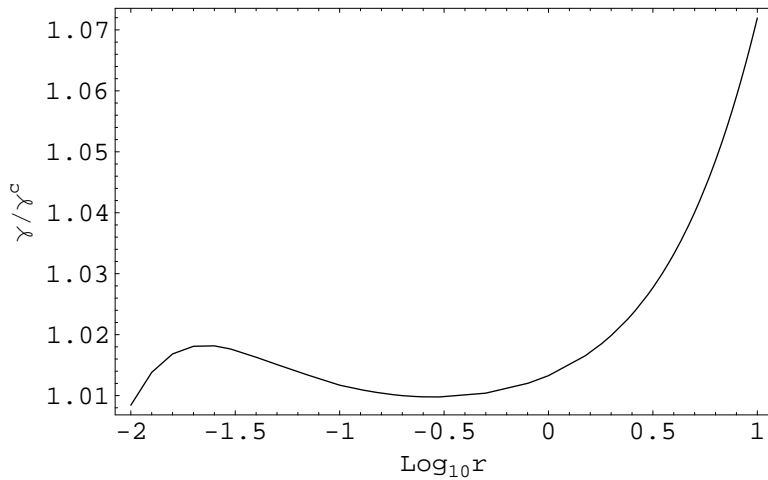


Figure 7. KH growth rate versus entropy ratio r for standard neutron star parameters (Case A) and zero viscosity, normalised to the classical growth rate ($\gamma^c = 1.77 \times 10^{15} \text{ s}^{-1}$ at $U = 10^6 \text{ m s}^{-1}$). The growth rate satisfies $\gamma \propto U^3 \sigma^{-1}$.

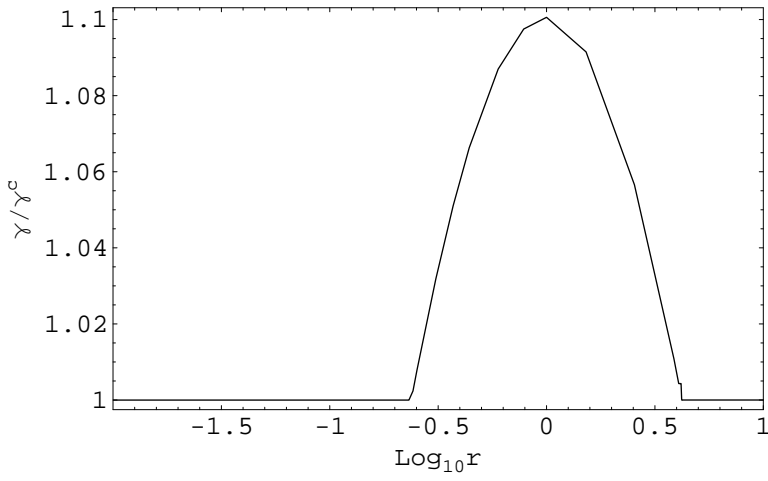


Figure 8. KH growth rate versus entropy ratio r for standard neutron star parameters (Case A), viscosity $\nu = 0.1 \text{ m}^2 \text{ s}^{-1}$, and zero surface tension, normalised to classical growth rate ($\gamma^c = 2.27 \times 10^{12} \text{ s}^{-1}$). The growth rate satisfies $\gamma \propto U^2 \nu^{-1}$.